Analysis of the Effectiveness on Reducing Welding Distortion of a Low Transformation Temperature Weld Wire

Adán Vega
Laboratorio Especializado en Procesos de Unión y Manufactura (LEPUM), Facultad de Ingeniería Mecánica, Universidad Tecnológica de Panamá
adan.vega@utp.ac.pa

Hidekazu Murakawa
Joining and Welding Research Institute, Osaka University, 11-1, Ibaraki, 567-0047, Japan
murakawa@jwri.osaka-u.ac.jp

David Dye, Miloslav Béres
Department of Mechanical Engineering, Imperial College London, London SW7 2AZ, UK
david.dye@imperial.ac.uk,
miloslav.beresm@dew-stahl.de

Abstract- *A three–dimensional numerical finite element model has been developed to predict the distortion pattern in butt welded specimens produced by welding of thin ferritic steel plates. The sensitivity of distortion to the filler metal used was examined using a conventional weld wire and a low transformation temperature weld wire. The model employed allows the effect of transformation start temperature (Ts) on distortion to be investigated. The results show that the usage of a low transformation temperature weld wire significantly reduces the weld distortion.*

Keywords- *(Solid–state phase transformation) (Displacive phase transformation) (Residual stress) (FEM) (Welding distortion)*

Resumen- *Un modelo tridimensional de elementos finitos ha sido desarrollado para predecir la distorsión producida por el proceso de soldadura de una lamina delgada de acero ferrítico. Dos tipos de materiales de aporte (un electrodo convencional y un electrodo de baja temperatura de transformación) fueron considerados y su influencia en la distorsión de la lámina soldada fue estudiada en detalle. El modelo desarrollado permite estudiar el efecto de la temperatura inicial de transformación en la distorsión de la lámina. Los resultados muestran que la distorsión producida por soldadura puede ser reducida considerablemente utilizando un electrodo de baja temperatura de transformación.*

Palabras Claves- *(Transformación de Fase en Estado Sólido) (Transformación de Fase No Difusiva) (Esfuerzo Residual) (Distorsión Producida por Soldadura) (Método de Elementos Finitos)*

Paper type: *Original*
Received: *January 24, 2011*
Accepted: *July 13, 2011*

1. INTRODUCTION

Over the past three decades, much progress has been made in developing numerical models for the thermal and mechanical stress and strain fields that develop around welds, with particular emphasis on the prediction of residual stresses [1]. However, the prediction of weld induced distortion has historically been more problematic, both because of a lack of understanding of the boundary conditions associated with the applied constraints and because of the difficulty of modelling buckling instability.

This is unfortunate because in many applications, such as shipbuilding, the control of distortion presents critical economic issues associated with the construction of large welded structures, for example the difficulty of fixturing and jigging presented by welding one welded assembly to another. Necessarily fabrication is often performed in field environments where process control is more problematic.

These conditions also limit the remedial measures, such as thermal tensioning, that can be taken to prevent distortion. In addition, any remedial approach should be capable of application to the full range of welding situations, e.g. to fillet and corner welds as well as to butt welds. Recently [2, 3], it has been suggested that the strain associated with phase transformations may be used to control the residual stresses and distortion that arise during welding, for instance by modification of the filler metals used in Gas Metal Arc Welding (GMAW).

However, for optimisation of the welding sequence and to develop an understanding of the transient stress fields that develop around the weld, it is desirable to be able to model the phase transformations, for example in a welding finite element simulation.

Recently, much progress has been made in this area in steels [4, 6], following on from early work on modelling the austenite → ferrite transformation during welding [7].

Of course, any weld model should in the first instance be validated against experimental data. First, the thermal conditions around the weld should be determined, typically using both thermocouples placed near the weld and the shape of the fusion zone. In addition the residual stresses can be characterised using incremental hole drilling, X–ray sin2ψ measurements, synchrotron X–ray or neutron diffraction [8, 9]. Finally the distortion itself can be characterised using, for example, photogrammetry or a co–ordinate measurement machine. Such validation provides confidence that any weld model developed may then be applied to varying plate geometries, enabling optimisation of the production sequence.

In the present paper, we develop a validated model for the GMA welding of thin ferritic steel plate using two types of filler metal, one with similar composition to the parent plate and one that easily undergoes a displacive phase transformation at relatively low temperatures on cooling of the weld metal, showing how the use of such filler metal leads to reduced distortion and lowered residual stresses in the weld.

2. WELDING TESTS

Weld trials were carried out to capture the characteristics of residual stress and distortion patterns generated in thin ferritic steel plates by GMAW procedure [10, 11]. The material chosen for base plate was a high strength low alloy DH–36 steel. In a trial, two plates of dimensions 500 mm long, 250 mm wide and 4 mm thickness were single pass butt welded. For filler material, two weld wires (1 mm in diameter) were used; one was a conventional weld wire (CW) which undergoes solid–state phase transformation at a relatively high temperature, 560 °C, and the other was the one with a low transformation temperature (LTT) i.e. 420 °C. The chemical compositions of the plates and the weld consumables are shown in Table 1. Nickel was the primary addition made to lower the transformation temperature in the LTT wire.

During manual welding the plates were rested, unclamped, on wooden pallets and held 4 mm apart by series of approximately 25 mm long tack welds at three locations with intervals of approximately 220 mm. A ceramic backing tile was used to contain the weld pool. The welding conditions employed are listed in Table 2. The overall heat input was nearly the same both welds manufactured.

During the welding trials the temperatures were measured at distances 7, 11.5 and 31 mm from the weld centre line as function of time using K–Type thermocouples. The thermocouples were spot welded on the top surface and measurements were conducted until the plates cooled down to room temperature.

After welding the residual stresses were analysed using neutron diffraction at the ILL, Grenoble, France using the SALSA diffractometer. These results have been previously reported [10, 12]. Post weld microstructural characterisation, distortion measurements, isothermal compression tests and dilatometric analysis on samples extracted from welded plates were conducted [13].

Table 1. Chemical composition (wt. %) of steel plate, conventional weld wire and LTT weld wire.

	C	Si	Mn	P	S	Cu	Ni	Cr	Nb
Steel plate	0.11	0.18	1.29	0.01	0.004	0.02	0.03	0.03	0.01
Conventional weld wire	0.07	0.61	1.42	0.01	0.01	0.14	0.04	0.02	0.02
LTT weld wire	0.04	0.32	0.36	0.008	0.004	0.15	11.9	-	-

Table 2. Welding conditions employed

	Weld speed [mm s^{-1}]	Weld current [A]	Weld voltage [V]	Heat input [kJ mm^{-1}]	Parameter Q/h^2 [J mm^{-3}]
CW	2.7	150	18	1.00	62.5
LTTW	3.5	180	20	1.03	64.3

3. MODELLING APPROACH

Numerical simulation to analyse the thermal–mechanical response to welding was carried out using the finite element code JWRIAN developed at JWRI, Osaka University. This is based on the iterative substructure method [14]. Three–dimensional models were constructed and only half of the welded plate was modelled, applying symmetry along the weld line. The plate thickness was divided into four equal sized mesh elements, 1 mm in depth. In the weld zone, three elements, 1

mm wide (normal to weld line) and 2.5 mm long (in the direction of the weld line), were used. In the region further away from weld zone a coarser mesh was adopted. The model contains 18,500 elements and 23,855 nodes. The same mesh was employed for both the thermal analysis and the thermo–mechanical analysis, with compatibility between the strain and temperature fields being enforced at the point of interpolation of the temperature results into the mechanical analysis. The exact shape of the weld bead and the use of tack welds were not taken into account.

In the present study, the simulations were carried out sequentially: first the thermal analysis and then the thermo–mechanical analysis. In the thermal analysis, the transient temperature fields in the plates during welding were solved. The results were then used in thermo–mechanical analysis to calculate displacements, strains and stresses. This was done using a finite element (FE) model that accounts for the solid–state phase transformation by computing the transformation and thermal strains [13]. Temperature dependent mechanical and thermo–physical properties of the weld metal, base metal and austenite phase were used in the model. Yield stress and thermal expansion of the materials were determined experimentally, whereas other properties including the Young's modulus and Poisson's ratio were obtained from [15]. The mechanical properties employed are shown in Figure 1. For heating cycle, properties of LLTW, CW and base metal were used whereas for cooling, only the properties of the austenite phase were used prior to transformation. During a phase transition, the law of mixtures were applied to mechanical properties of the welded region and heat affected zone (HAZ) in order to take into account the different volume fraction of each phase [13].

In general, buckling of a perfectly flat plate under in–plane loading occurs instantaneously when the critical buckling load is reached. This is critical when performing computation involving buckling distortion. At the buckling load, it is difficult for finite element method (FEM) algorithms to find the buckled stable configuration and so often they continue to follow the unstable unbuckled configuration. To avoid such situation, usually a small amount of initial deflection is applied such that the FEM algorithm can follow the deflected shape and predict buckling. Very small load increments are required in the vicinity of the buckling load in order to obtain a correct solution.

In welding, the tendon force in the fusion zone (FZ) and heat affected zone cause compressive stresses in the plate outside the HAZ that may lead to buckling when welding thin plates. In the FEM analysis, these welding deformations provide the displacements that lead to the prediction of buckling by the FEM algorithm. However, depending on the state of deformation when the buckling load is reached, the welded plate can buckle in any direction; the system is unstable to perturbations. This makes comparison of different welding conditions difficult if buckling occurs in different directions in different trials. Therefore, in the present simulations, an initial upward angular deformation of 0.1 mm at the plate edges was defined in the plates to be welded. This allowed the buckling distortion to consistently occur in an upwards direction.

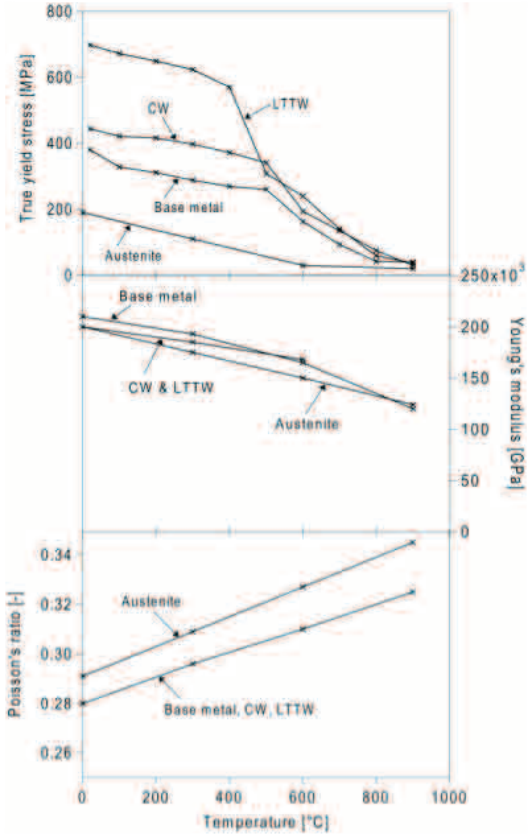

Figure 1. Temperature dependent mechanical properties employed in the computation for the a) yield stress, b) Young's modulus and c) Poisson's ratio [15]

The temperature dependent values used for specific heat capacity, material density and thermal conductivity for all materials and phases are shown in the Figure 2. [16]. A non–uniform heat flux was applied through the thickness with a volumetric heat source of dimensions 10 mm (length) × 3 mm (half–width) × 4 mm (depth). The total net heat input per unit length, Q, was described by the relationship:

$$Q = \eta IV/v \quad (1)$$

where η is the thermal efficiency, V and I are the weld torch voltage and current, respectively, and v the welding speed. A thermal efficiency, η = 0.6, was determined by matching the thermal analysis results to the experimental thermocouple measurements. By doing so, the wall–plug heat input was taken to be 0.60 kJ mm^{-1} for the conventional wire and 0.62 kJ mm^{-1} for the LTT wire. Convection and radiation heat transfer boundary conditions were employed at all plate surfaces and edges except along the symmetry plane where adiabatic conditions were applied. To account for heat losses through convection and radiation following relationship was used:

$$Qloss = h\,\Delta T \quad (2)$$

where $Qloss$ is the heat flux loss, h is the combined convection and radiation heat transfer coefficient and ΔT is the difference between surface and ambient temperature. The value of h was determined by comparing the computed thermal profile with the experimentally obtained thermal profile measurements during welding and subsequent cooling. The temperature dependence of the heat transfer coefficient is shown in the Figure 2. Mechanical constraints were applied at the symmetry plane and edge of the plate. The plate was allowed to deform freely; however rigid body motions were restrained.

4. RESULTS AND DISCUSSION

The residual stress distribution in the welded plate should be known before modelling the distortion. The modelling results showed the presence of a compressive longitudinal stress of around -120 MPa at the weld centre line, Figure 3(a). This prediction agrees well with the measurements in the LTT wire (dashed lines). However the predicted transverse stresses for LTT wire are lower than those determined experimentally, especially near the fusion zone. The normal stresses were found to be small in both the modelling and experimental results, as expected for a thin plate.

In order to examine the effect the transformation start temperature, Ts, on the resulting residual stresses and distortion, a number of analyses have been performed by considering both the actual filler materials and various hypothetical fillers exhibiting a range of transformation start temperatures. The longitudinal stress prediction at the centre line at the plate mid–length is shown in Figure 3 (b). As Ts decreases, the stress near the weld centre line reduces and becomes compressive when Ts falls below 430 °C. The stress reaches a minimum (max. compressive value) of approximately -690 MPa when the Ts temperature is lower than 150 °C.

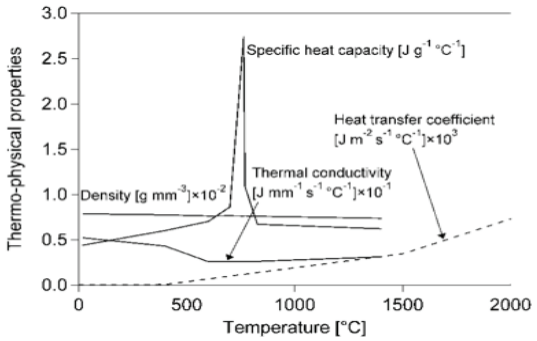

Figure 2. Temperature dependent thermo–physical properties and heat transfer coefficient employed for all materials and phases.

Figure 4 shows predicted contours of out of plane displacement at the top surface of the plate for the LTT wire with Ts of 420 °C. Mechanical constraints were applied: Points A and A" were restrained in the direction normal to the plate and in addition point A was restrained in the welding direction. The model was a half model, so at the symmetry plane at the weld centre line all elements were restrained in the transverse direction. The predicted out of plane displacement was greatest at the end of the weld, point B".

The distortion butterfly angle between the two sides of the plate along the lines ABC and A"B"C" was also measured, Table 3. Again, a

reduction on the order of 10 % in distortion is observed for the LTT wire compared to the CW, which is also predicted by the model. Here, model and experiment are in good agreement. Overall, the butterfly distortion is under–predicted by a similar factor to the over–prediction in the camber distortion mode, a phenomenon often observed in under determined buckling problems. Importantly, the trends between the LTT and CW cases are reproduced in magnitude and sign.

Table 3. Butterfly distortion in the plates (angle subtended along paths A–B–C, A''–B''–C'', in degrees).

	Start (A–B–C)		End (A''–B''–C'')		Average	
	CW	LTT	CW	LTT	CW	LTT
Experiment	4.0	3.7	6.2	5.3	5.1	4.5
Model	3.3	3.1	4.7	3.8	4.0	3.4

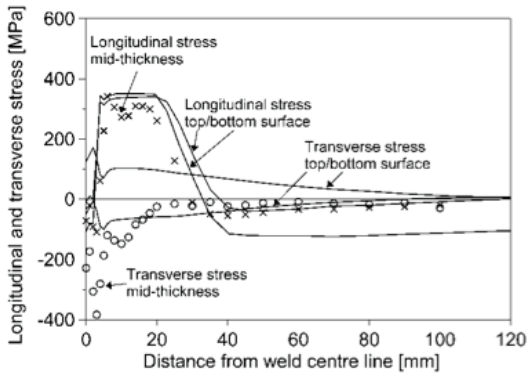

(a)

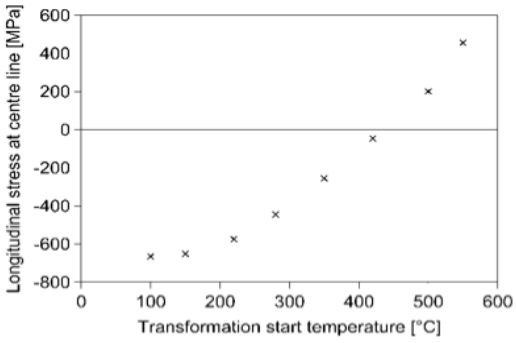

(b)

Figure 3. a) Comparison of computed longitudinal and transverse stresses (lines) with neutron diffraction measurements (points); b) predicted relationship between the longitudinal residual stress over range of transformation start temperature in the plate mid–thickness at the weld centre line [13].

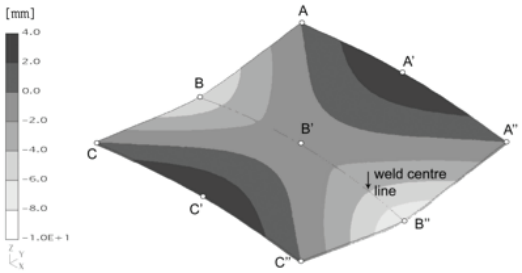

Figure 4. Predicted out of plane displacements for the model employing the LTT wire properties with Ts = 420 °C, where B denotes start, B'' end of welding, A' mid length at the plate edge and B' mid length at the weld centre line.

Figure 5. (a) shows the variation in out of plane displacement along the line B' – A' at different stages before, during and after welding for Ts = 420 °C. Initially, the plate is undistorted. However, as mentioned previously, in order to overcome the buckling instability problem, the initial angular distortion at A' is taken to be 0.1 mm (stage 0). At stage 1 – when the torch has just passed B', the plate begins to distort. Maximum distortion in the negative direction takes place at B'. Towards end of welding, stage 2, the distortion continues in the negative direction and B' has moved further to -1.4 mm. Between stage 1 and 3, negative displacement at the weld line (marked by B'), and relatively small and negative displacements at plate edge (marked by A') are caused by transverse angular distortion.

In cooling stage at around 250 °C i.e. at stage 3, the displacement along A' – B' starts to increase, and at the end of cooling (i.e. stage 4), the region near A' becomes positively displaced and region near B' remains negatively displaced. At this stage, a large curvature along the B' – A' is observed and the magnitude of the final distortion at the plate edge (of which A' is the mid–point) is twice that on the centre line (of which B' is the mid–point). Since the increase in displacement between stage 3 and 4 is not induced by transverse angular distortion (and no lateral loads that are suddenly applied to the plate and can cause such displacement were induced), it can be concluded that it is the result of buckling.

Figure 5. (b) shows the change in out of plane displacement as a function of (arbitrary) time at points A', B' and B''. At stage 1, when the torch approaches B', the region in vicinity of B' starts to displace negatively and remains negatively displaced to the end of cooling (stage 4). A variation of between 0 and 2 mm in the magnitude

of displacement was predicted at that point. From stage 1 up to stage 3, the displacements of the regions in vicinity of A' and B'' remain nearly constant and negative, and do not exceed 1 mm in magnitude. However, when the cooling commences (i.e. at around 250 °C), a sudden change of displacement is observed, as B'' displaces to -8 mm and A' to +4 mm. This indicates the occurrence of buckling distortion during cooling. This trend is observed only when large distortions are considered in the analysis.

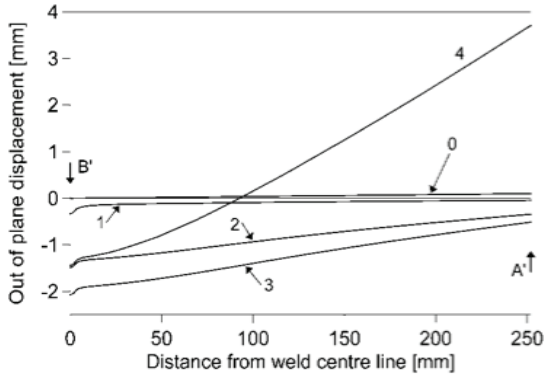

(a)

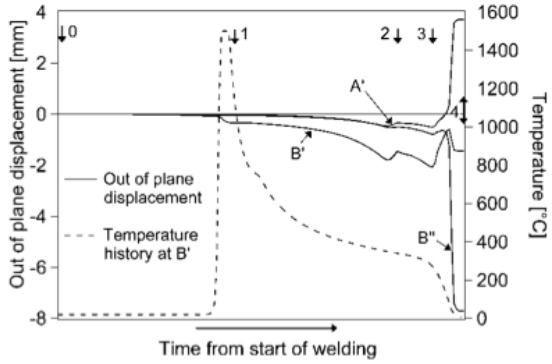

(b)

Figure 5. Evolution of out of plane displacement predictions for LTT wire (Ts = 420 °C) a) at mid–length between A' and B', b) for individual points A', B', B'' at the mid–length and edge, together with the temperature at B'. Stage 0 – start of welding, 1 – torch just passed B', 2 – end of welding, 3 – during cooling at around 250 °C and 4 – end of cooling.

Transverse shrinkage was also examined as it is one of the fundamental dimensional changes that occur during welding and can induce distortion in fabricated structures [1]. Figure 6 shows the variation in transverse shrinkage as a function of distance from the weld centre line for different transformation temperatures. For this purpose, the point marked D was selected, 15 mm from the weld centre line, because due to rotation of the plate around the weld centre line (angular distortion) it is difficult to evaluate the effect of initial distortion on transverse shrinkage by considering a point at the plate edge. At D it can be assumed that only local shrinkage occurs and that the effect of plate rotation is negligible.

The results presented in Figure 6 shows that as Ts increases, the transverse shrinkage at point D decreases. In the fusion zone (FZ) and adjacent heat affected zone (HAZ), the shrinkage is accommodated plastically. As Ts decreases, the thermal strain imposed during cooling prior to transformation increases and so the shrinkage due to plasticity also increases, from 0.26 to 0.29 mm. The peak values at this point are plotted in Figure 7 as function of transformation temperature. The transverse shrinkage attains a maximum value of 0.29 mm at Ts ~ 280 °C. From this maximum value, the transverse shrinkage starts to decline with further reductions in Ts.

Three mechanisms can be identified that affect this behaviour:

(i) The transformation expansion, assumed to occur isotropically.

(ii) The coefficient of thermal expansion of the different phases, giving rise to different amounts of thermal strain to be accommodated. Since a phase–dependent thermal expansion coefficient was used in the numerical model and the expansion coefficient of austenite is larger than that of acicular ferrite, a lower Ts temperature results in a greater extent of shrinkage produced in the weld metal before cooling to Ts.

(iii) The relative stiffness of the FZ and HAZ during transformation. As the weld metal in the FZ and parent metal in the HAZ cools down, the relative material stiffness and strength in these two zones differs with temperature. When transformation takes place at high temperature, the weld material expansion in the longitudinal direction will be restricted by the HAZ (which is at a lower temperature and has higher strength and stiffness). The longitudinal transformation expansion is then changed into transverse positive (expansive) plastic strain. This causes the transverse shrinkage to decrease. As the transformation temperature decreases, the stiffness and strength of the FZ gradually becomes

closer to that of the HAZ. Therefore the HAZ can only restrict the FZ longitudinal expansion to a reduced extent and the expansive transverse plastic strain becomes less. Further, due to Poison's ratio (0.5 for plasticity), the longitudinal positive strain resulting in the HAZ is accompanied by transverse shrinkage. The decrease in transverse shrinkage becomes less than that when the transformation occurs at high temperature.

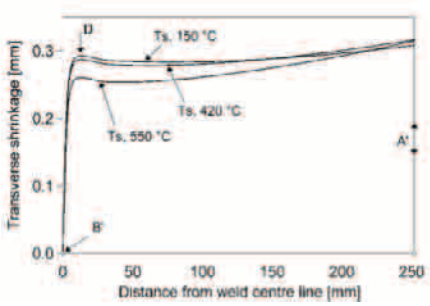

Figure 6. Transverse shrinkage predicted for a range of transformation start temperatures.

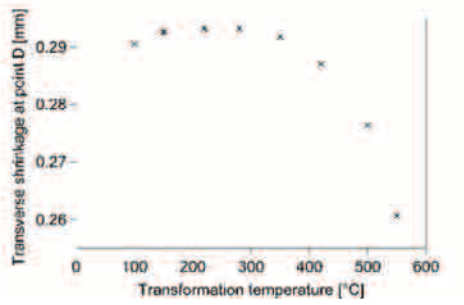

Figure 7. Relationship between maximal transverse shrinkage and transformation start temperatures at point "D", 15 mm from weld centre line.

Overall, dependence of transverse shrinkage on transformation start temperature depends on the relative magnitude of these three. Table 4 summarizes the cases that have been considered. In all cases in Table 4 the austenite start temperature, As, was set to 630 °C and the austenite finish temperature, As, was set to 770 °C.

Experimentally, initial distortion is observed to have a profound effect on the as–welded final distortion. Several computations evaluating the influence of initial angular distortion on the residual distortion were carried out. Initial angular distortion varied between 0.1 mm and 5 mm as shown in Table 5.

Figure 8 indicates that there is only a slight decline in additional distortion (distortion due to welding) with the increase of initial angular distortion.

Table 4. Details of the cases examined, where Ts denotes the transformation start temperature on cooling and Tf the transformation finish temperature.

Case	Ts [°C]	Tf [°C]	Longitudinal stress at point B' [MPa]	Displacement at point A' [mm]	Transverse shrinkage at point C [mm]
1	550	450	456	4.27	0.261
2	500	400	201	4.12	0.277
3	420	320	-46	3.73	0.287
4	350	250	-255	3.58	0.292
5	280	180	-445	3.50	0.293
6	220	120	-575	3.28	0.293
7	150	50	-651	3.15	0.293
8	100	0	-665	3.15	0.291

Table 5. Summary of cases examined when considering initial angular distortion for a transformation start temperature of 420 °C.

Case	10	11	12	13	14	15	16	17	18
Initial angular distortion [mm]	0.10	0.25	0.50	0.75	1.00	2.00	3.00	4.00	5.00
Final camber distortion [mm]	3.73	3.72	3.72	3.71	3.68	3.51	3.36	3.20	3.08
Transverse shrinkage [mm]	0.287	0.287	0.286	0.284	0.282	0.276	0.271	0.266	0.262

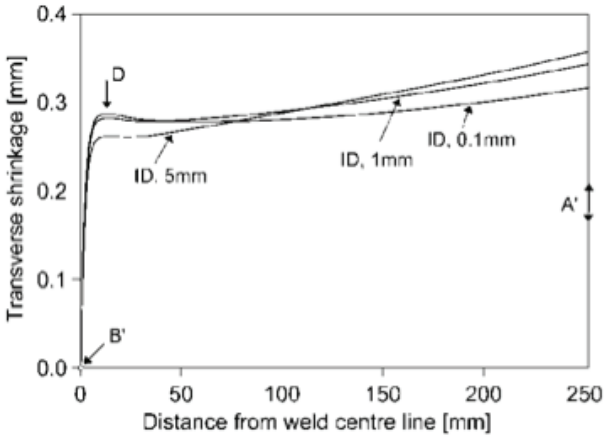

Figure 8. Variation in transverse shrinkage at the plate mid–length, where "ID" denotes initial angular

distortion in mm.

5. CONCLUSIONS

A three–dimensional numerical finite element model has been used to predict the distortion pattern in butt welded specimens produced by GMA welding of thin ferritic steel plates. The sensitivity of distortion to the filler metal used was examined using a conventional weld wire and a low transformation temperature (LTT) weld wire.

The model employed calculates the phase transformation strain in addition to the thermal strain, allowing the effect of transformation start temperature (Ts) on distortion to be investigated.

The transient evolution of distortion was analysed. The following conclusions can be drawn from this work

1. The proposed FE model is capable of predicting both the residual stresses pattern and the distortion observed.
2. The results indicate that a Ts below 400 °C results in compressive residual stresses in the fusion zone. Generally, a reduced Ts leads to lower residual stresses in the weld region and consequently to a substantial reduction in distortion.
3. Fairly good quantitative agreement between the calculated and experimental results was achieved.
4. Transient distortion analysis revealed that the majority of the camber distortion arises towards end of cooling, after welding is complete.
5. Transverse shrinkage was explained as function of Ts and initial angular distortion.

6. ACKNOWLEDGEMENTS

This research was partially support by the Panamanian Secretary of Science and Technology (SENACYT), through a grant for International Collaboration (APY-GC10-044 A-2010). Their contribution is greatly appreciated.

7. REFERENCES

[1] Masubuchi, K., Analysis of welded structures: residual stresses, distortion, and their consequences, 1980: Pergamon Press, Oxford.

[2] Bhadeshia, H., Possible effects of stress on steel weld microstructures, Institute of Materials, Mathematical Modelling of Weld Phenomena 2, 1995(United Kingdom), pp. 71-118.

[3]Bhadeshia, H., Developments in martensitic and bainitic steels: Role of the shape deformation, Materials Science and Engineering A-Structural Materials Properties Microstructure and Processing, 2004, 378(1-2), pp. 34-39. 10.1016/j.msea.2003.10.328

[4] Deng, D., Hidekazu, M. and Yukihiko, H., FEM Simulation of Welding Residual Stress in Multi-pass Butt-welded Modified 9Cr-1Mo Steel Pipe Considering Phase Transformation Effects, Transactions of JWRI, 2004, 33(2), pp. 167-176.

[5] Deng, D., FEM prediction of welding residual stress and distortion in carbon steel considering phase transformation effects, Materials & Design, 2009, 30(2), pp. 359-366.

[6] Mikami, Y., Morikage, Y., Mochizuki, M. and Toyoda, M., Angular distortion of fillet welded T joint using low transformation temperature welding wire, Science and technology of welding and joining, 2009, 14(2), pp. 97.

[7] Leblond, J. B., Devaux, J. C., Mottet, G. and Devaux, J., Mathematical models of anisothermal phase transformations in steels, and predicted plastic behaviour, Materials Science and Technology; MST, 1984, 1(10), pp. 815-822.

[8] Stone, H. J., Withers, P. J., Roberts, S. M., Reed, R. C. and Holden, T. M., Comparison of three different techniques for measuring the residual stresses in an elecltron beam-welded plate of Waspaloy, Metallurgical and Materials Transactions; A; Physical Metallurgy and Materials Science, 1999, 30A(7), pp. 1797-1808.

[9] Jensen M.V.R.S., Dye D., James K.E., Korsunsky A.M., Roberts S.M. and Reed R.C., Residual stresses in a welded superalloy disc: Characterization using synchrotron diffraction and numerical process modeling Metallurgical and Materials Transactions A, 2002, 33(9), pp. 2921-2931.

[10] Davies, C. M., Béreš, M., Hughes, D., Dye, D. and Nikbin, K. M., The Influence of Geometric and Welding Parameters on Residual Stress in Thin Welded Steel

Structures, in Proceedings of PVP2009 ASME Pressure Vessels and Piping Division Conference, July 26th-30th 2009, Prague, Czech Republic.

[11]Davies, C. M., Wimpory, R. C., Béreš, M., Lightfoot, M. P., Dye, D., Oliver, E., O'Dowd, N. P., Bruce, G. J. and Nikbin, K. M., The Effect of Residual Stress and Microstructure on Distortion in Thin Welded Steel Plates, in Proceedings of PVP2007 ASME Pressure Vessels and Piping Division Conference, July 22-26, 2007, San Antonio, Texas.

[12]Davies, C. M., Wimpory, R. C., Dye, D. and Nikbin, K. M., The effect of plate dimensions on residual stresses in welded thin steel plates, in Proceedings of the ASME Pressure Vessels and Piping Conference - 2008 Vol. 6, 2009, Amer Soc Mechanical Engineers, New York, pp. 309-319.

[13]Murakawa, H., Béreš, M., Davies, C., Rashed, S., Vega, A.,Tsunori, M., Nikbin, K., Dye, D., The Effect of Low Transformation Temperature Weld Filler Metal on Welding Residual Stress, submitted for Science and Technology of Welding & Joining in February 2010.

[14]Nishikawa, H., Serizawa, H. and Murakawa, H., Actual application of FEM to analysis of large scale mechanical problems in welding, Science and technology of welding and joining, 2007, **12**(2), pp. 147-152. 10.1179/174329307x164274

[15]Bhadeshia, H. K. D. H., Handbook of Residual Stress and Deformation of Steel, Eds. G.E. Totten, M.A.H. Howes, T. Inoue, ASM International, 2002.

[16]Tsunori, M., Davies, C. M., Dye, D. and Nikbin, K. M., Numerical Modelling of Residual Stress and Distortion in Thin Welded Steel Plates, in Proceedings of PVP2008 ASME Pressure Vessels and Piping Division Conference, July 27th-31st 2008, Chicago, Illinois, USA.